RSC Advances

ROYAL SOCIETY OF CHEMISTRY

www.rsc.org/advances

Gallic acid magnetic nanoparticles for photocatalytic degradation of meloxicam: Synthesis, characterization and application to pharmaceutical wastewater treatment

Ahmed H. Nadim[a], Medhat A. Al-Ghobashy[a,b,*], Marianne Nebsen[a] and Mostafa A. Shehata[a]

[a] Analytical Chemistry Department, Faculty of Pharmacy, Cairo University, Egypt

[b] Bioanalysis Research Group, Faculty of Pharmacy, Cairo University, Egypt

[*]**Correspondence:**

Dr. Medhat A. Al-Ghobashy, Analytical Chemistry Department, Faculty of Pharmacy, Cairo University, Cairo 11562, Egypt

E-mail: medhat.alghobashy@cu.edu.eg

Keywords:

Gallic acid magnetic nanoparticles; Pharmaceutical waste water treatment; Cleaning validation; RP-HPLC; Photodegradation

Abstract

Environmentally friendly gallic acid coated magnetic nanoparticles (GA-MNP) have been synthesized and evaluated as a novel photocatalyst for degradation of Meloxicam; a commonly prescribed nonsteroidal anti-inflammatory drug. The synthesized GA-MNP were characterized using transmission electron microscopy (TEM), Fourier transform infrared (FTIR) spectroscopy and dynamic light scattering. Results showed the formation of core-shell MNP with a mean hydrodynamic diameter of 160.55 ±5.02 nm and zeta potential of -42.4 ±1.6 mV. A validated RP-HPLC stability-indicating assay was developed for monitoring of Meloxicam concentration in the presence of its degradation products and for determination of the kinetics of degradation. Full factorial design (2^4) was employed in order to investigate the effects of pH, irradiation time, GA-MNP loading and initial Meloxicam concentration on the efficiency of the process. The irradiation time was found the most significant parameter followed by initial Meloxicam concentration and GA-MNP loading, respectively. At the optimized conditions, increasing GA-MNP loading to 5.00 mg/mL demonstrated superior photocatalytic activity when compared to bare MNP and TiO_2NP. Meloxicam degradation was found to follow pseudo first order rate kinetics with K_{obs} and $t_{0.5}$ of -0.0029 min^{-1} and 239 min respectively. The protocol was successfully applied for treatment of incurred water samples collected during various cleaning validation cycles. A percentage degradation of 89.10 ± 0.13% was achieved upon irradiation of samples containing 64.57 ± 0.09 µg/mL with UV light (1012 µW/cm^2, 8 h) in the presence of 5 mg/mL GA-MNP at pH 9.0 ± 0.05. It could be suggested that treatment of waste waters collected during the cleaning validation of each pharmaceutical product, before pooling into the general waste pool, should improve the efficiency and economics of pharmaceutical waste water treatment.

1. Introduction

Pharmaceutical compounds are one of the most important classes of environmental pollutants continuously discharged into waste water [1]. Inefficient treatment of pharmaceutical waste water has led to frequent detection of pharmaceutical compounds in water resources such as sewage effluents, surface water, ground water and drinking water [2]. Meloxicam (MELO), a commonly used enol carboxamide NSAIDs (Fig. S1) has been detected in river water, influent and effluent of waste water treatment plants despite of its poor water solubility[3-5]. This was attributed to the use of alkaline washing solutions for cleaning production lines that increase the aqueous solubility of MELO up to 17.90 mg/mL at pH 10.7 [6]. Various methods for the analysis of MELO in pharmaceutical dosage forms and biological fluids have been reported such as spectrophotometry [7], spectrofluorimetry [8], TLC-densitometry [7], polarography [9], liquid chromatography [10, 11] and capillary electrophoresis [12]. However, the determination of MELO in aquatic samples and in the presence of its photodegradation products has been limited to tandem mass spectrometric methods[3-5, 13].

In order to avoid the undesired accumulation of pollutants such as pharmaceuticals in aquatic environments, filtration, adsorption, coagulation-flocculation, flotation [14] and electrochemical techniques such as anodic oxidation, electro-oxidation with active chlorine, electro-Fenton, photoelectron-Fenton and photoelectrocatalysis [15-17] were employed. On the other hand, advanced oxidation processes (AOPs) have shown a great potential for the degradation of hazardous pollutants [18]. Photocatalysis, based on the use of TiO_2 nanoparticles (TiO_2NP) represents one of the most extensively investigated AOPs for removal of organic pollutants [19]. However, there are many limitations regarding TiO_2NP efficiency such as high recombination rate of photo-induced electrons and holes, difficulty of separation from treated water after each

run and adsorption of some reaction products (CO_2 and H_2O) on the surface of TiO_2 in the gas-solid photocatalyst system [20-22].

Recently, the synthesis and utilization of iron oxide magnetic nanoparticle (MNP) have been widely studied in many environmental applications. This could be attributed to the high surface area to volume ratios, superparamagnetism, low toxicity, chemical inertness and biocompatibility of MNP [23, 24]. They have been applied as a photocatalyst in waste water treatment either alone [25], in combination with noble metal [26], in photo-Fenton like system with oxalate [27] or as a sensitizer of TiO_2 [28]. However, bare MNP were found susceptible to atmospheric oxidation and aggregation in aqueous systems. Thus, suitable coatings were essential in order to overcome such limitations [29]. Core shell NP with inner magnetic core and outer surface modifications using different organic compounds such as citric acid [30] and humic acid [31] have been reported.

Gallic acid (GA) is one of the main constituents of herbal roots and tea leaves, a natural product of tannin hydrolysis and one of the simplest dissolved organic matter in natural water with antioxidant and pro-oxidant effects (Fig. S1) [32, 33]. Several methods have been reported for GA degradation such as electrochemical [34], UV/air, UV/Fe^{3+} /air, UV/Fe^{3+}/N_2 [35], UV/TiO_2 [32], UV/H_2O_2, photo-Fenton [36] and ozonation [37]. It has been reported that UV irradiation of GA under aerobic conditions can lead to the generation of reactive oxygen species (ROS) and hydrogen peroxide [35, 36]. In addition, Sun and Pignatello reported the photodegradation of pesticides using Fenton's reaction of hydrogen peroxide and soluble Fe^{3+}- GA chelate [38]. Thus, it could be suggested that the incorporation of GA as a coat for MNP will not only increase the stability of NP but also its efficiency in photodegradation of organic pollutants. The synthesis of gallic acid magnetic nanoparticles (GA-MNP) for drug delivery and therapeutic applications has

been reported[39-42]. However, to the best of our knowledge the use of GA-MNP as a photocatalyst in waste water treatment has not been reported.

In this study, environmentally friendly core shell GA-MNP have been synthesized, characterized and used for treatment of pharmaceutical waste water containing MELO. A validated RP-HPLC assay has been developed for monitoring of MELO throughout the treatment process. Optimization of the photocatalytic degradation process was achieved using full factorial design and the kinetics of MELO degradation was calculated. Application to incurred waste water collected during the cleaning validation was suggested as an economic alternative to treatment of pooled pharmaceutical waste water.

2. Materials and methods

2.1. Chemicals and samples

Iron (II) chloride tetrahydrate, GA and TiO_2NP (surface area >14.0 m^2/g, Cat. No. 677469) were purchased from Sigma-Aldrich (USA). Iron (III) chloride hexahydrate was purchased from Alpha Chemika (India). MELO reference standard (purity 100.02% ± 0.42) and waste water samples were kindly supplied by ADWIA Pharmaceuticals (Egypt). All other chemicals were of HPLC grade and were obtained from Sigma-Aldrich (USA). Incurred water samples collected at different stages of the cleaning validation process were obtained: i) first wash of production lines using an alkaline detergent (Tergajet, Alconox, USA) and ii) second and third washes using water.

2.2. Instruments

UV irradiation was carried out using a calibrated UV lamp (Vilber Lourmat, France) housed in an air ventilated cabinet. A transmission electron microscope (TEM 2100; JEOL, Japan) was used to collect TEM images of GA-MNP. Fourier transform infrared (FTIR) spectroscopy was

performed using JASCO FT-IR 1600 (Japan). Particle size distribution and zeta potential were measured using Zetasizer Nano ZS-ZEN 3600 (Malvern Instruments Ltd, UK). The system is controlled with DTS Nano ver. 6.12 software and is equipped with 4 mW helium/neon laser at 633 nm wavelength and measurements are conducted using noninvasive backscatter technology at a detection angle of 173° (Malvern instruments Ltd, UK). The experimental design and the statistical analysis of the results were carried out using Minitab 2010, ver. 16.1.1 (Minitab Inc., USA). Chromatographic separations were carried out using Agilent 1200 HPLC system controlled with Chemstation software (Agilent Technologies, Germany).

2.3. Synthesis and characterization of NP

2.3.1 Bare MNP

Bare MNP were prepared by facile co-precipitation method as previously described with slight modifications [29, 42]. Briefly, 6.4% $FeCl_2.4H_2O$ and 15.1% $FeCl_3.6H_2O$ were prepared by dissolving 0.64g $FeCl_2.4H_2O$ and 1.51g $FeCl_3.6H_2O$ in 10 mL degassed water using vortex mixer. The solution was heated to 80 °C for 15 min with shaking and 10 mL of 7.5% ammonia solution were added drop wise. The mixture solution was further heated at the same temperature for 15 min with shaking. The supernatant containing bare MNP was vacuum dried at 60 °C after centrifugation at 7000 rpm for 20 min.

2.3.2 GA-MNP

Iron solution was prepared as described above and equal volume of gallic acid solution (0.2% w/v prepared in degassed water) was added and heated in water bath at 80 °C for 15 min with shaking. An aliquot of 20 mL of 7.5% ammonia solution was added drop wise to the iron-gallic acid mixture while heating at 80°C for 15 min with shaking. Aggregates were removed by

centrifugation at 7000 rpm for 20 min and the supernatant was collected and dried under vacuum at 60 °C.

2.3.3 Characterization of MNP and GA-MNP

The morphology of the synthesized nanoparticles was inspected using TEM. One drop of the sample was placed on a copper grid and left to dry in air, then examined at 160 kV. The formation of GA coat onto MNP has been confirmed using FTIR. Samples were compacted with KBr (approximately 1%), analyzed in transmission mode and the obtained spectra were examined for the characteristic bands. The mean diameter and particle-size distribution were determined using dynamic light-scattering with a Zetasizer at 25 °C. Samples were diluted ten times with water and measured in duplicate. Results were presented as an average diameter of the GA-MNP (z-average mean) against percent sample intensity, and the polydispersity index (PDI); a measure of the width of the size distribution was also deduced. The average zeta potential was determined in duplicate using the Zetasizer at 25 °C for 120 seconds using a combination of laser doppler velocimetry and phase-analysis light scattering to measure particle electrophoretic mobility. The hydrodynamic size and the zeta potential of GA-MNP has also been investigated following UV irradiation in order to assess the stability of the organic coat as will be described below.

2.4. Reversed phase liquid chromatography

A previously developed HPLC assay was used in order to determine MELO in the presence of its photodegradation products and calculate the kinetics of degradation [43]. Briefly, analysis was conducted using Zorbax Eclipse XDB – C18 column, 4.6 × 250.0 mm, 5.0 µm (Agilent Technologies, USA). The mobile phase composition was 50 mM diammonium hydrogen phosphate buffer (pH 8.0 ± 0.05): methanol: acetonitrile (40:50:10 v/v/v). Isocratic elution was

employed at a flow rate of 1.0 mL/min and detection was achieved at 364 nm. An aliquot of MELO standard solution (25 mL, 100 µg/mL in phosphate buffer pH 9.0) was subjected to UV irradiation 1012 µW/cm^2 for 8 h in the presence of 5 mg/mL GA-MNP in order to prepare MELO photodegraded sample. This sample was analyzed as described and system suitability parameters were calculated according to US Pharmacopoeia[44]. A set of MELO standard solutions was prepared over a concentration range of 200 – 20000 ng/mL and analyzed. Calibration curve was constructed and the obtained regression equation was used to calculate the concentration of residual MELO throughout the study. Validation was performed to pharmaceutical industry standards according to ICH guidelines[45].

2.5 Photocatalytic degradation study

2.5.1 Preliminary studies

Two standard MELO samples (500.00 µg/mL) were prepared in phosphate buffer pH 9.0 and pH 11.0 and were stored at room temperature, away from light for up to 30 h and the hydrolytic stability was assessed. A preliminary study was then carried out in order to investigate the capability of GA-MNP as a photocatalyst. Four standard MELO samples (250.00 µg/mL) were prepared in phosphate buffer (pH 9.0) and were subjected to UV irradiation (254 nm, 1012 µW/cm^2, 4h) and results were compared to those obtained upon irradiation of equivalent samples in the presence of: i) bare MNP (12 mg/mL), ii) GA solution (2 mg/mL) and iii) GA-MNP (12 mg/mL). At the end of the incubation period, samples were analyzed using HPLC assay as described.

2.5.2 Experimental design

The effects of pH, irradiation time, GA-MNP loading and initial MELO concentration on the efficiency of MELO photocatalyzed degradation process were investigated. Two levels for each

of the four factors (2^4) were arbitrarily assigned either as low (−1) or high (+1), as shown in Table 1. Sixteen sets of experimental conditions (2^4, full factorial design) in addition to two center points were performed (Table 2). Throughout this study, aliquots of 25 mL of buffered MELO solution and GA-MNP were placed in a set of Petri dishes then irradiated using UV light as specified in each experiment (Table 2). All experiments were carried out at room temperature, in air ventilated cabinet while continuously stirred. At the end of the incubation period, samples were completed to volume (25 mL), suitably diluted and filtered through 0.2 µm syringe filter then analyzed using the HPLC assay. Results were calculated relative to the results of an equivalent control sample that has not been subjected to UV irradiation.

2.5.3. Kinetics of MELO photocatalytic degradation

The kinetics of MELO photocatalytic degradation reaction was investigated over 4 h at the optimum set of degradation conditions: MELO (100.00 µg/mL, pH 9.0 and UV light intensity1012 µW/cm^2) in presence of GA-MNP (5 mg/mL). The gradual decrease in MELO concentration over time was monitored using the RP-HPLC assay.

2.6 Application to incurred samples

Following the production of one batch of MELO tablets, cleaning validation was conducted according to the pre-approved protocol (Egyptian Drug Authority, Ministry of Health, Egypt). Three washing cycles were performed using a commercially available alkaline wash solution Tergajet, Alconox, USA (Cycle 1) and purified water (Cycles 2 and 3). Pooled samples collected throughout each cycle were stored at - 20 ^{o}C after recording its pH. Initial MELO concentration was then determined in triplicate, pH was adjusted to ~ 9.0 and samples were irradiated with UV light (1012 µW/cm^2) in the presence of GA-MNP (5 mg/mL) for up to 8 h. At the end of the irradiation period, MELO concentration was determined and the percentage degradation was

calculated. GA-MNP were then recovered, re-suspended and the hydrodynamic size and zeta potential were measured.

3. Results and discussion

In this study, GA has been selected as a model for naturally occurring polyphenolic compounds as discussed above. This class of compounds was previously used to provide a protective coat for various types of NP [42, 46, 47] and to generate ROS upon UV irradiation [35, 36]. Here, GA-MNP were synthesized and their potential use as a catalyst in photocatalytic degradation of MELO in industrial waste water has been investigated. MELO was selected on the basis of its relative photostability [13, 43] thus process optimization was crucial.

3.1 Synthesis and characterization of NP

An eco-friendly GA-MNP were prepared using a simple co-precipitation method. Neither complex surfactants nor hazardous reducing agents were used. An economic, naturally occurring coating agent (GA) was employed due to its high affinity towards iron oxide MNP [42] and ability to generate ROS upon UV irradiation [35, 36]. GA contains one reactive carboxyl group and three phenolic groups per molecule and can easily form an organic layer on the surface of nanoparticles [48]. The GA coating shell was thus expected to enhance the stability as well as the catalytic activity of MNP.

The morphology of NP was visualized using TEM and results were compared to those obtained using bare MNP. In the absence of GA coat, MNP suffered from aggregation (Fig. 1A). TEM images of GA-MNP showed spherical, well separated and dispersed core-shell NP with some agglomeration (Fig. 1B). This was attributed to the presence of the protective organic coat formed of GA. These results were in agreement to the previously reported data about the role of GA and other organic materials for reducing aggregate formation[42, 46, 47].

FTIR spectra of bare MNP (Fig. 2A) and GA-MNP (Fig. 2C) showed peaks at 564 - 611 cm^{-1} that are characteristic for the stretching vibration of Fe-O-Fe in MNP [49]. Pure GA (Fig. 2B) showed a band at 1707 cm^{-1} for C=O stretching of COOH group and broad bands in the range of 2800 – 3500 cm^{-1} for both carboxylic and phenolic –OH groups [42]. GA-MNP (Fig. 2C) showed C-O band at 1402 cm^{-1}along with the broad phenolic –OH band. This indicated the formation of a covalent C-O bond and confirmed the formation of GA coat onto MNP surface.

It is well known that zeta potential measurements can be used to provide useful information about surface charges as well as the colloidal stability of NP [50]. Magnetite is an amphoteric solid and thus can develop both positive and negative charges on its surface due to protonation ($FeOH + H^+ \rightarrow FeOH^{2+}$) and deprotonation ($FeOH + H^+ \rightarrow FeO^- + H^+$) of FeOH sites generated on surface of magnetite when dispersed in water [51]. In this study, zeta potential measurements were carried out at the alkaline medium (pH 11.0) used for synthesis of NP. Results revealed that bare MNP and GA-MNP had zeta potential of -22.15 ±1.20 mV and -42.4 ±1.6 mV, respectively. The higher zeta potential of GA-MNP could be attributed to the ionization of the phenolic hydroxyl groups in the capping moieties at alkaline pH [46, 52] and indicated good coating of iron surface cations through O-Fe linkage [53]. The high negative charge formed a repulsive barrier that helped avoid aggregation and improved the colloidal stability of GA-MNP. This was clearly reflected on the hydrodynamic size of bare MNP (283.65±2.33, PDI 0.64±0.13) and GA-MNP (160.55 ±5.02 nm, PDI 0.52 ±0.03).

3.2. Reversed phase liquid chromatography

A photodegraded MELO sample was prepared as described and used during the development and validation of the HPLC assay. Good resolution was obtained over 5 min using 50 mM diammonium hydrogen phosphate buffer (pH 8.0): methanol: acetonitrile (40:50:10 v/v/v) as the

mobile phase (Fig. 2). Results were compared to those obtained using an equivalent control sample that has not been subjected to UV irradiation in order to confirm the identity of MELO and calculate the percentage degradation. System suitability parameters were calculated according to the US Pharmacopoeia and separation efficiency was demonstrated (Table 3). A linear relationship was obtained between the integrated peak area and MELO concentration over a concentration range of 200 – 20000 ng/mL. Regression equation and validation parameters are summarized in Table 3.

3.3. Photocatalytic degradation study

3.3.1 Preliminary studies

Initially, the hydrolytic stability of MELO at pH 9.0 – 11.0 was confirmed at room temperature over 30 h. (data not shown). This experiment was conducted in order to ensure that the decrease in MELO concentration achieved upon UV irradiation was solely due to the effect of light. The efficiency of the photocatalytic activity of GA-MNP was demonstrated using a set of MELO control samples (250.00 µg/mL, pH 9.0) subjected to UV irradiation for 4 h. In the absence of any photocatalyst, a percentage degradation of approximately 5% was achieved. While in the presence of: i) bare MNP (12 mg/mL), ii) GA solution (2 mg/mL) and iii) GA-MNP (12 mg/mL), percentage degradation of 10%, 16% and 25% were noted, respectively. These results were in agreement to the previously reported data showing the relative photostability of MELO [13, 43], photocatalytic activity for bare MNP [25] and the prooxidant effect of GA in the presence of UV light [35]. Results obtained using GA-MNP (12 mg/mL) were 15% higher than those noted with bare MNP. This could be attributed to the fast rate of electron-hole charge recombination that occurs at the surface of bare MNP [23]. The presence of GA coat could facilitate the transfer of surface electrons leading and separation between electrons and holes leading to better efficiency.

This finding is supported by the previously reported role of GA as a source of ROS upon UV irradiation [35, 36] and in capturing charge carriers when adsorbed onto TiO_2 films [54].

3.3.2 Experimental design

Further investigations were carried out in order to optimize the effects of (A) pH, (B) irradiation time, (C) GA-MNP loading and (D) initial MELO concentration on the efficiency of MELO photocatalyzed degradation. These factors were chosen considering the previously reported designs in the literature [30, 55]. It should be noted that a relatively narrow range of pH 9.0 – 11.0 was studied for the following reasons: **i)** poor solubility of MELO in aqueous media below pH 7.0 and **ii)** detergent solutions commonly used in MELO cleaning validation are of alkaline nature. Full factorial design was employed to assess the relative significance of each factor, interactions as well as the optimum set of experimental conditions required to optimize the performance of MELO degradation (Table 1). Samples were analyzed in duplicate using RP-HPLC assay and percentage degradation was determined (Table 2).

3.3.3 Analysis of the results

Analysis of the full factorial design results was carried out at 95% confidence level (P 0.05) using the percentage degradation as the response factor. Pareto diagram is used to compare the relative magnitude of the studied factors as well as the interactions between them. The direction of effects is obtained from the normal plot of the standardized effects. A positive effect indicates an increase in the studied response at high levels of the respective variables; while a negative effect indicates an increase in the response at low levels of these variables, within the studied range [56, 57].

In this study, irradiation time (B) and GA-MNP loading (C) were found of significant impact with a positive effect while initial MELO concentration (D) was significant but with a negative

effect (Fig. 4 and Fig. S2). It should be noted that the interactions BC (irradiation time - GA-MNP loading) and BCD (irradiation time - GA-MNP loading – initial MELO concentration) showed no significant effect but with P values of 0.055 and 0.059, respectively as shown in Fig. 4 and summarized in Table S1. The effect of pH was found non-significant that could be attributed to the limited solubility of MELO below pH 7.0 which hindered the extension of the studied pH range. It could be concluded that the longer the irradiation time and the higher the GA-MNP loading, the more degradation observed. In addition, irradiation of samples containing low initial concentrations of MELO should require lower energy and improve the efficiency and economics of the water treatment process.

The combined effects of the significant factors (time, GA-MNP loading and initial concentration) were also graphically demonstrated using 3D surface plot. Figure 5 demonstrated clearly that although each of the studied factors had a significant main effect, the combined effects (interactions) had no significant effect. Such results confirmed the need of thorough statistical analysis of the results while optimizing the performance of such complex process.

Based on the obtained results, it could be suggested that free radical-mediated MELO photodegradation occurs via: i) production of ROS such as H_2O_2, $O_2^{\cdot-}$ and $^{\cdot}OH$ upon UV irradiation of GA coat [36], ii) interaction of ROS; liberated upon UV irradiation of water sample containing GA-MNP with GA leading to the formation of phenoxyl radicals [58] and iii) intrinsic enzyme mimetic activity exhibited by MNP; similar to that found in peroxidases that catalyze the formation of ROS from H_2O_2 [59, 60].

The regression equation summarizing the experimental design is given as follows:

$$Y= -84.21 + 16.80\,A + 13.07\,B + 56.39\,C + 0.36\,D - 1.88\,AB - 7.01\,AC - 0.07\,AD - 5.28\,BC - 0.01\,BD - 0.25\,CD + 0.81\,ABC + 0.01\,ABD + 0.03\,ACD + 0.02\,BCD - 0.01ABCD$$

where Y = %degradation, A = pH, B = irradiation time, C = GA-MNP loading and D = initial MELO concentration.

ANOVA was carried out and results were summarized in Table S1. The response value (%degradation) obtained from the experimental data and that calculated from the model were found in agreement, as summarized in Table 2.

Further investigations were carried out in order to compare the efficiency of GA-MNP to that of commercially available TiO_2NP. Two Standard MELO solutions (250.00 µg/mL) were prepared using phosphate buffer (pH 9.0) and subjected to UV irradiation (1012 µW/cm^2) for 8 h in the presence of 0.8 mg/mL of either TiO_2NP or GA-MNP. Percentage degradation of 41.51% and 38.72% were obtained with TiO_2NP and GA-MNP, respectively. Although these results might indicate approximately the same efficiency for both types of particles, our results indicated that increasing TiO_2NP loading had no significant effect on the efficiency of MELO degradation [43]. This observation was previously demonstrated on the basis of reaching a plateau region above 0.4 – 0.8 mg/mL [22, 43, 61]. On the other hand, statistical analysis of the factorial design results showed clearly the positive effect of increasing GA-MNP concentration (Fig. 4). Thus, higher GA-MNP loadings (up to 5 mg/mL) were employed in application to incurred samples, as will be discussed below.

3.4. Kinetics of MELO degradation

The kinetics of photodegradation was studied using the set of experimental conditions that resulted in 66.66% degradation (Table 2). This value corresponded to a MELO initial concentration of 100.00 µg/mL prepared in buffer of pH 9.0 and irradiated with UV light intensity of 1012 µw/cm^2 for 8 h in the presence of 5 mg/mL GA-MNP. Upon plotting $\ln(C_t/C_o)$ versus time, a straight line was obtained that indicated a pseudo-first order kinetics ($r > 0.98$)

(Langmuir–Hinshelwood model) with K_{obs} and $t_{0.5}$ of -0.0029 min^{-1} and 239 min, respectively (Fig. 6). This model has been widely considered as the basis for photodegradation of organic compounds [22, 53]. Results obtained using GA-MNP were found superior to those obtained in the presence of 0.4 mg/mL TiO_2NP (K_{obs} -0.0009 min^{-1} and $t_{0.5}$ 770 min) [43]. Thus, it could be concluded that the faster kinetics observed using GA-MNP should improve the economics of MELO photodegradation process.

3.5 Application to incurred samples

Incurred samples were collected during Cycle1 of the cleaning validation process and MELO concentration was determined (64.57 ± 0.09 µg/mL). On the other hand, samples collected during Cycle 2 and Cycle 3 were evaporated under vacuum and MELO concentration was found to be 0.09 ± 0.01 µg/mL and below the LOQ in Cycle 2 and Cycle 3 samples, respectively. The applicability of the developed photocatalyzed degradation protocol was then investigated using Cycle 1 samples. Treatment was carried out as described and percentage degradation of 89.10 ± 0.13% and 88.74 ± 0.27% were noted with incurred and control samples, respectively. Lack of matrix interference was confirmed by the absence of significant difference in the percentage degradation. Following to one cycle of UV irradiation for 8 h, GA-MNP were recovered and the zeta potential and hydrodynamic size were measured and compared to those obtained before UV irradiation. Results showed that the zeta potential decreased from -42.4 ± 1.6 mV to -28.3 ± 3.71 mV while the mean hydrodynamic size was found to increase from 160.55 ± 5.02 nm to 215.40 ± 4.87 nm. These results confirmed the contribution of GA in generating the ROS and maintaining the stability of GA-MNP as discussed above. Results were also compared to those obtained using 0.4 mg/mL TiO_2NP and percentage degradation of 76.34 ± 0.02% was obtained [43]. These results

showed better efficiency of GA-MNP as a photocatalyst in the pharmaceutical waste water treatment.

4. Conclusion

Eco friendly GA-MNP were synthesized and employed as a novel catalyst in the photodegradation of pharmaceutical waste water containing MELO. A validated RP-HPLC testing protocol was described to monitor residual MELO concentration during treatment processes. Full Factorial design approach was successfully employed in order to understand various factors affecting performance of MELO photocatalytic degradation process. The most influencing parameters were irradiation time, initial concentration and GA-MNP loading. The kinetics of MELO photocatalytic degradation followed pseudo first order model. The treatment protocol was successfully applied for incurred samples collected during the cleaning validation process. GA-MNP showed superior photocatalytic properties over bare MNP and it could be used as a green, cost-effective alternative to TiO_2NP. Pooling of waste water fractions obtained throughout the cleaning validation should also reduce MELO concentration and further improve the efficiency of photocatalyzed degradation using GA-MNP.

References

1. C. Gadipelly, A. Perez-Gonzalez, G. D. Yadav, I. Ortiz, R. Ibanez, V. K. Rathod and K. V. Marathe, *Ind. Eng. Chem. Res.*, 2014, **53**, 11571-11592.
2. D. Fatta-Kassinos, S. Meric and A. Nikolaou, *Anal. Bioanal. Chem.*, 2011, **399**, 251-275.
3. M. Gros, S. Rodríguez-Mozaz and D. Barcelo, *J. Chromatogr. A*, 2012, **1248**, 104-121.
4. M. Petrovic, B. Skrbic, J. Zivancev, L. Ferrando-Climent and D. Barcelo, *Sci. Total Environ.*, 2014, **468**, 415-428.
5. L. Zhao, N. Liang, X. Lun, X. Chen and X. Hou, *Anal. Methods*, 2014, **6**, 6956-6962.
6. N. Seedher and S. Bhatia, *AAPS PharmSciTech*, 2003, **4**, 36-44.
7. M. Starek and J. Krzek, *Talanta*, 2009, **77**, 925-942.
8. E. M. Hassan, *J. Pharm. Biomed. Anal.*, 2002, **27**, 771-777.
9. S. Altınoz, E. Nemutlu and S. Kır, *Il Farmaco*, 2002, **57**, 463-468.
10. J.-W. Bae, M.-J. Kim, C.-G. Jang and S.-Y. Lee, *J. Chromatogr. B*, 2007, **859**, 69-73.
11. T. Velpandian, J. Jaiswal, R. K. Bhardwaj and S. K. Gupta, *J. Chromatogr. B*, 2000, **738**, 431-436.
12. E. Nemutlu and S. Kir, *J. Pharm. Biomed. Anal.*, 2003, **31**, 393-400.
13. D. T. Modhave, T. Handa, R. P. Shah and S. Singh, *Anal. Methods*, 2011, **3**, 2864-2872.
14. V. K. Gupta, I. Ali, T. A. Saleh, A. Nayak and S. Agarwal, *RSC Adv.*, 2012, **2**, 6380-6388.
15. M. Carballa, F. Omil and J. M. Lema, *Water Res.*, 2005, **39**, 4790-4796.
16. I. Sires and E. Brillas, *Environ. Int.*, 2012, **40**, 212-229.
17. X. Qu, P. J. Alvarez and Q. Li, *Water Res.*, 2013, **47**, 3931-3946.
18. S. Malato, J. Blanco, A. Vidal and C. Richter, *Appl. Catal. B: Environmental*, 2002, **37**, 1-15.
19. M. N. Chong, B. Jin, C. W. Chow and C. Saint, *Water Res.*, 2010, **44**, 2997-3027.
20. W. Wu, C. Jiang and V. A. Roy, *Nanoscale*, 2015, **7**, 38-58.
21. F. Han, V. S. R. Kambala, M. Srinivasan, D. Rajarathnam and R. Naidu, *Appl. Catal. A: General*, 2009, **359**, 25-40.
22. U. I. Gaya and A. H. Abdullah, *J. Photochem. Photobiol. C: Photochem. Rev.*, 2008, **9**, 1-12.
23. P. Xu, G. M. Zeng, D. L. Huang, C. L. Feng, S. Hu, M. H. Zhao, C. Lai, Z. Wei, C. Huang and G. X. Xie, *Sci. Total Environ.*, 2012, **424**, 1-10.
24. S. C. Tang and I. M. Lo, *Water Res.*, 2013, **47**, 2613-2632.
25. M. Khedr, K. A. Halim and N. Soliman, *Mater. Lett.*, 2009, **63**, 598-601.
26. C.-T. Wang, *J. Non-Cryst. Solids*, 2007, **353**, 1126-1133.
27. J. Lei, C. Liu, F. Li, X. Li, S. Zhou, T. Liu, M. Gu and Q. Wu, *J. Hazard. Mater.*, 2006, **137**, 1016-1024.
28. M. S. Lucas, P. B. Tavares, J. A. Peres, J. L. Faria, M. Rocha, C. Pereira and C. Freire, *Catal. Today*, 2013, **209**, 116-121.
29. R. Kaur, A. Hasan, N. Iqbal, S. Alam, M. K. Saini and S. K. Raza, *J. Sep. Sci.*, 2014, **37**, 1805-1825.
30. D. Singh, R. K. Gautam, R. Kumar, B. K. Shukla, V. Shankar and V. Krishna, *J. Water Process Eng.*, 2014, **4**, 233-241.
31. L. Peng, P. Qin, M. Lei, Q. Zeng, H. Song, J. Yang, J. Shao, B. Liao and J. Gu, *J. Hazard. Mater.*, 2012, **209**, 193-198.
32. N. Quici and M. I. Litter, *Photochem. Photobiol. Sci.*, 2009, **8**, 975-984.
33. G.-C. Yen, P.-D. Duh and H.-L. Tsai, *Food Chem.*, 2002, **79**, 307-313.
34. B. Boye, E. Brillas, A. Buso, G. Farnia, C. Flox, M. Giomo and G. Sandona, *Electrochim. Acta*, 2006, **52**, 256-262.
35. Y. Du, H. Chen, Y. Zhang and Y. Chang, *Chemosphere*, 2014, **99**, 254-260.

36. F. J. Benitez, F. J. Real, J. L. Acero, A. I. Leal and C. Garcia, *J. Hazard. Mater.*, 2005, **126**, 31-39.
37. M. Carbajo, F. Beltran, F. Medina, O. Gimeno and F. Rivas, *Appl. Catal. B: Environ.*, 2006, **67**, 177-186.
38. Y. Sun and J. J. Pignatello, *J. Agric. Food Chem.*, 1993, **41**, 308-312.
39. D. Dorniani, M. Z. B. Hussein, A. U. Kura, S. Fakurazi, A. H. Shaari and Z. Ahmad, *Int. J. Nanomedicine*, 2012, **7**, 5745.
40. M. Szekeres, E. Illes, C. Janko, K. Farkas and I. Toth, *J Nanomed Nanotechnol*, 2015, **6**.
41. M. Rahmayanti and S. J. Santosa, *Adv. Mater. Res.*, 2015, **1101**, 286-289.
42. I. Y. Toth, M. Szekeres, R. Turcu, S. Saringer, E. Illes, D. Nesztor and E. Tombacz, *Langmuir*, 2014, **30**, 15451-15461.
43. A. H. Nadim, M. A. Al-Ghobashy, M. Nebsen and M. A. Shehata, *Environ. Sci. Pollut. Res.*, 2015, 1-10.
44. The United States Pharmacopoeia & National Formulary (2011)
45. ICH Guidelines: Q2(R1) Validation of analytical procedures (2005)
46. A. A. AbdelHamid, M. A. Al-Ghobashy, M. Fawzy, M. B. Mohamed and M. M. S. A. Abdel-Mottaleb, *ACS Sustainable Chem. Eng.*, 2013, **1**, 1520-1529.
47. P. Panneerselvam, N. Morad and K. A. Tan, *J. Hazard. Mater.*, 2011, **186**, 160-168.
48. E. Tombacz, I. Toth, D. Nesztor, E. Illes, A. Hajdu, M. Szekeres and L. Vekas, *Colloids Surf. A Physicochem. Eng. Asp.*, 2013, **435**, 91-96.
49. T. T. Baby and S. Ramaprabhu, *Talanta*, 2010, **80**, 2016-2022.
50. V. Ayala, A. P. Herrera, M. Latorre-Esteves, M. Torres-Lugo and C. Rinaldi, *J. Nanopart. Res.*, 2013, **15**, 1-14.
51. L. Giraldo, A. Erto and J. C. Moreno-Piraján, *Adsorption*, 2013, **19**, 465-474.
52. M. A. Al-Ghobashy, *Bull. Faculty Pharm. CU*, 2014, **52**, 71-78.
53. V. Ayala, A. P. Herrera, M. Latorre-Esteves, M. Torres-Lugo and C. Rinaldi, *J. Nanopart Res.*, 2013, **15**, 1-14.
54. P. Z. Araujo, P. J. Morando, E. Martínez and M. A. Blesa, *Appl. Catal. B: Environ.*, 2012, **125**, 215-221.
55. K. P. Singh, A. K. Singh, U. V. Singh and P. Verma, *Environ. Sci. Pollut. Res.*, 2012, **19**, 724-738.
56. A. L. Giraldo, G. A. Penuela, R. A. Torres-Palma, N. J. Pino, R. A. Palominos and H. D. Mansilla, *Water Res.* , 2010, **44**, 5158-5167.
57. Y. Lin, C. Ferronato, N. Deng, F. Wu and J.-M. Chovelon, *Appl. Catal. B: Environmental*, 2009, **88**, 32-41.
58. N. Quici, M. I. Litter, A. M. Braun and E. Oliveros, *J. Photochem. Photobiol. A Chem.*, 2008, **197**, 306-312.
59. H. Wei and E. Wang, *Anal. Chem.*, 2008, **80**, 2250-2254.
60. L. Gao, J. Zhuang, L. Nie, J. Zhang, Y. Zhang, N. Gu, T. Wang, J. Feng, D. Yang and S. Perrett, *Nat. Nanotechnol.*, 2007, **2**, 577-583.
61. L. Yang, L. E. Yu and M. B. Ray, *Water Res.*, 2008, **42**, 3480-3488.

Tables

Table 1: Actual factors and their levels used for two-level full factorial design experiment.

Factor name	**Factor code**	**Low level (-1)**	**High level (+1)**
pH	A	9.0	11.0
Time (h)	B	4.0	8.0
GA-MNP loading (mg/mL)	C	2	5
Initial MELO concentration (µg/mL)	D	100.00	200.00

Table 2: Design matrix for 2^4 for full factorial design employed for MELO photocatalytic degradation and results obtained using the RP-HPLC assay.

Run No.	Factor code				RP-HPLC		
					MELO concentration (µg/mL)	% Photo-degradation	
	A	B	C	D		Exp*	Calc**
1	0	0	0	0	83.01	44.66	44.15
2	-1	+1	+1	+1	104.91	47.55	47.63
3	+1	-1	+1	-1	53.82	46.18	46.23
4	0	0	0	0	84.70	43.53	43.76
5	+1	-1	+1	+1	136.15	31.92	32.00
6	-1	-1	-1	-1	58.36	41.64	41.72
7	+1	-1	-1	+1	144.36	27.82	27.90
8	-1	-1	+1	+1	134.5	32.75	32.83
9	-1	+1	-1	+1	112.39	43.80	43.88
10	+1	-1	-1	-1	56.9	43.10	43.17
11	+1	+1	-1	+1	121.36	39.32	39.40
12	-1	+1	-1	-1	50.12	49.88	49.99
13	+1	+1	+1	+1	109.48	45.26	45.34
14	+1	-1	+1	-1	63.66	36.34	36.42
15	-1	-1	-1	+1	143.01	28.49	28.57
16	+1	+1	+1	-1	35.07	64.93	65.00
17	-1	+1	+1	-1	33.34	66.66	66.74
18	+1	+1	-1	-1	51.55	48.45	48.53

* Calculated relative to the results of an equivalent control sample that has not been subjected to UV light irradiation.

** Theoretically calculated by Minitab software using regression model

Table 3: Summary of system suitability and validation parameters for the proposed RP-HPLC assay

System suitability parameters	
Resolution (R)	7.57
Peak Symmetry	0.68
Relative retention time (α)	1.36
Column Capacity (K)	2.66
Number of theoretical plates (N)	21090.37
HETP (Height Equivalent to a Theoretical Plate)	0.0119
Validation parameters	
Accuracy (mean ± SD)	99.21 ± 1.07 [a]
Precision: Repeatability [b] Intermediate precision [c]	 98.57 ± 0.72 98.84 ± 1.00
Linearity Regression equation Correlation coefficient (r) Range	 Y = 0.0665C + 2.387 1.000 200 – 20000 ng/mL
LOD	120 ng/mL
LOQ	200 ng/mL

[a] Average percentage recovery of nine determinations

[b] The intraday, average of nine determinations over three concentration levels repeated within the same day

[c] The inter-day, average of nine determinations over three concentration levels repeated over three different days.

Figure captions

Figure 1: Transmission electron micrograph of bare MNP (A) and GA-MNP (B)

Figure 2: FTIR spectra of bare MNP (A), Pure GA (B) and GA-MNP (C)

Figure 3: HPLC Chromatogram showing the photocatalytic degradation of MELO (100 µg/mL) upon exposure to UV light intensity (1012 µW/cm2) at pH 9 for 8 hours in the presence of 5 mg/mL GA-MNP (B) compared to MELO control sample not subjected to UV light (A)

Figure 4: (A) Pareto chart of the standardized effects of single and interaction factors on % MELO photodegradation. (B) Normal plot of the standardized effect of single and interaction factors on % MELO photodegradation

Figure 5: 3D surface plot of % MELO photodegradation versus GA-MNP loading - time (A), initial concentration - GA-MNP loading (B) and initial concentration - time (C)

Figure 6: Kinetic profile of the photodegradation of 100.00 µg/mL initial MELO concentration at pH 9 with 5 mg/mL GA-MNP under UV irradiance of 1012 µw/cm2 analyzed by RP-HPLC assay

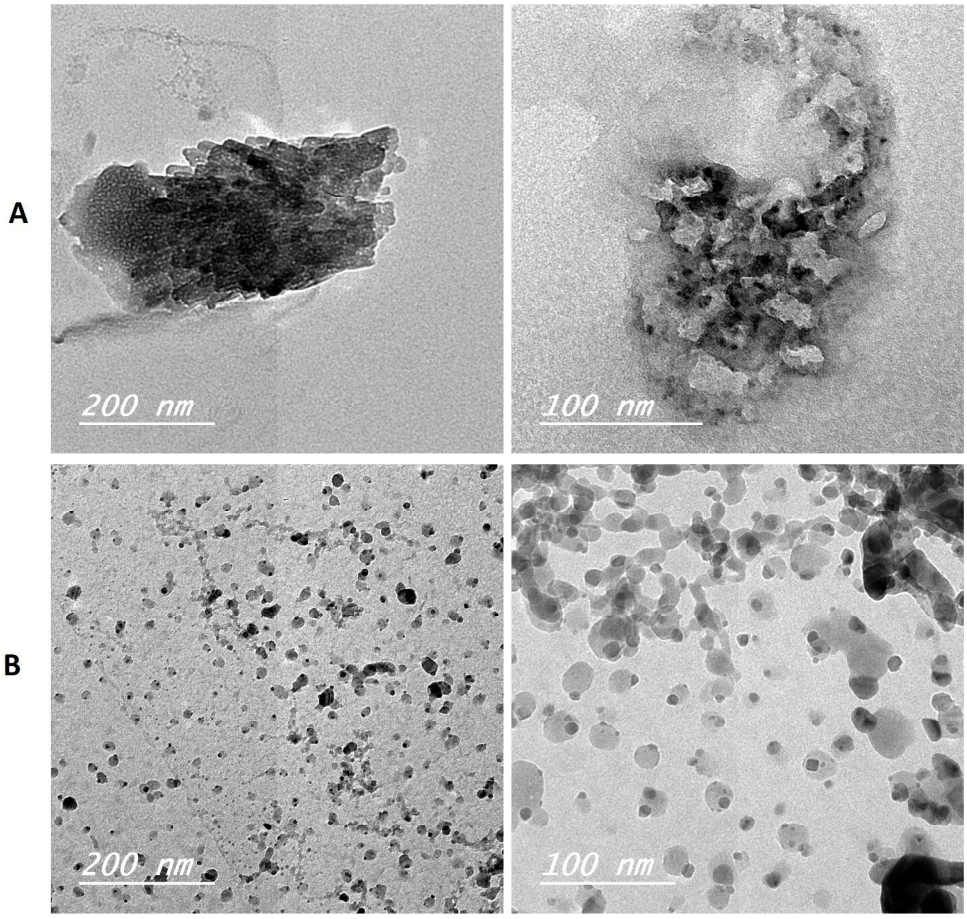

787x740mm (96 x 96 DPI)

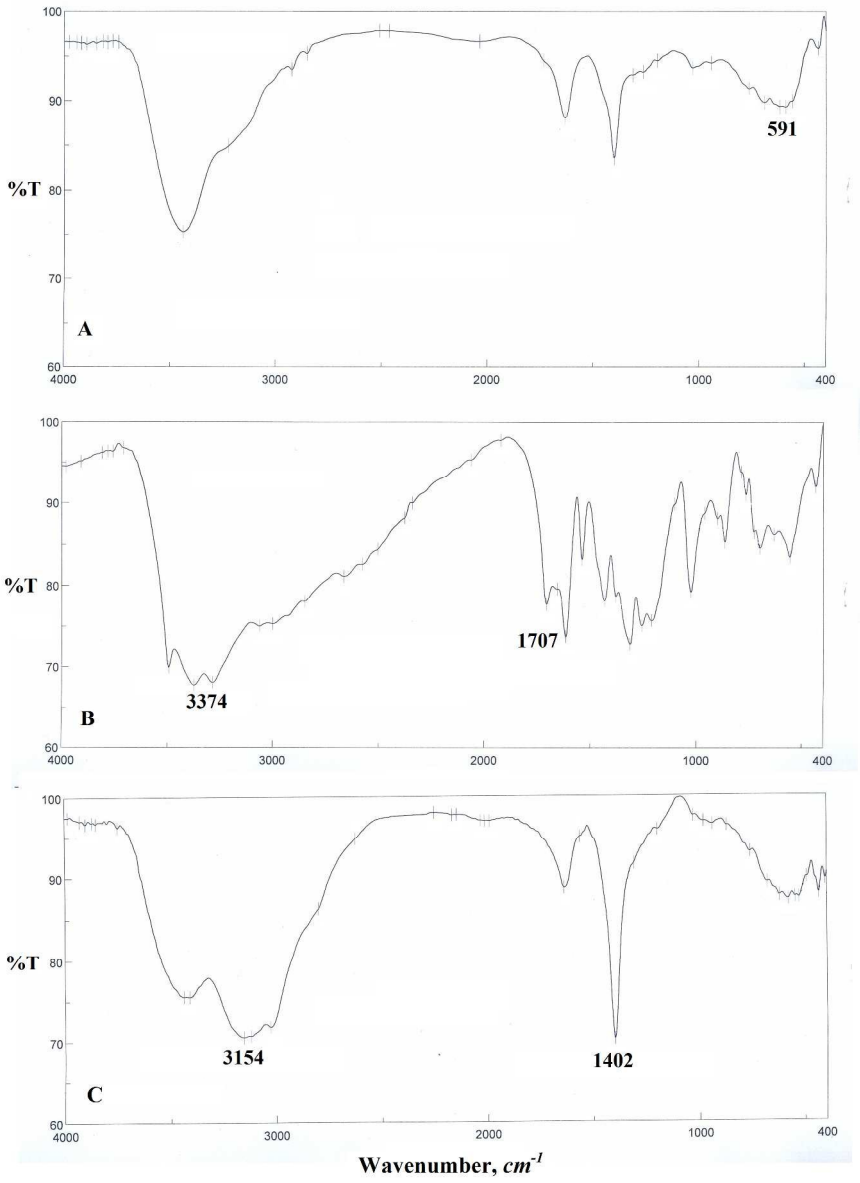

804x1111mm (96 x 96 DPI)

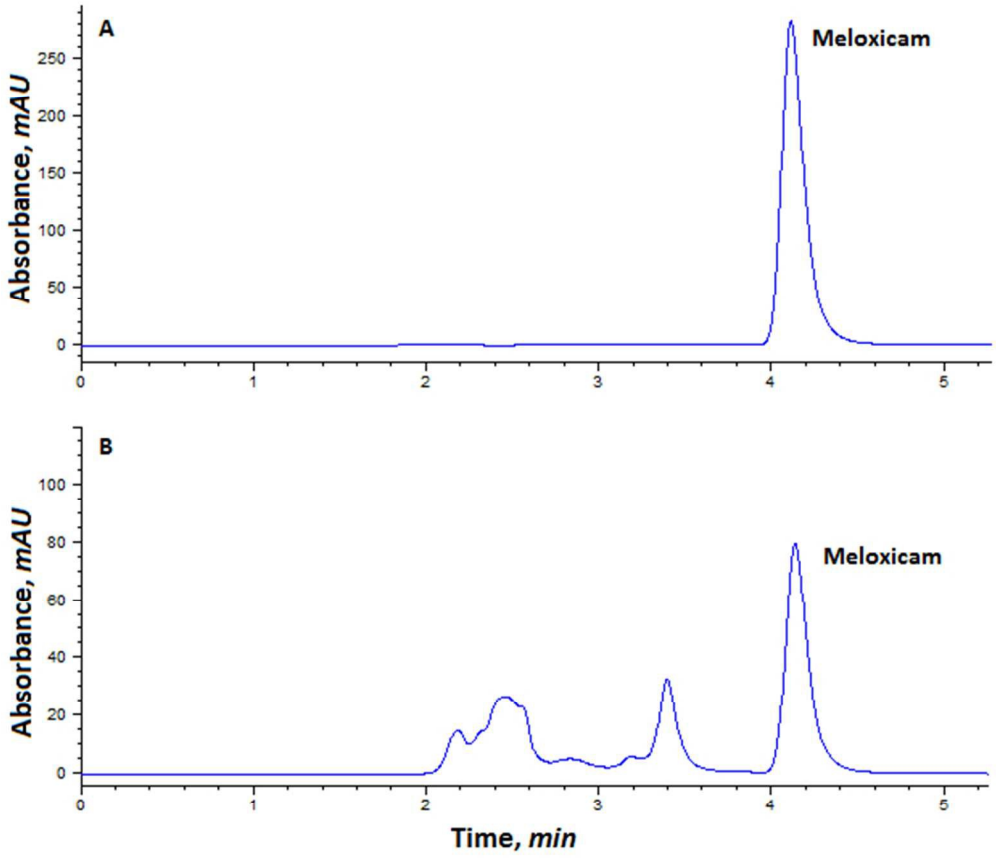

164x148mm (96 x 96 DPI)

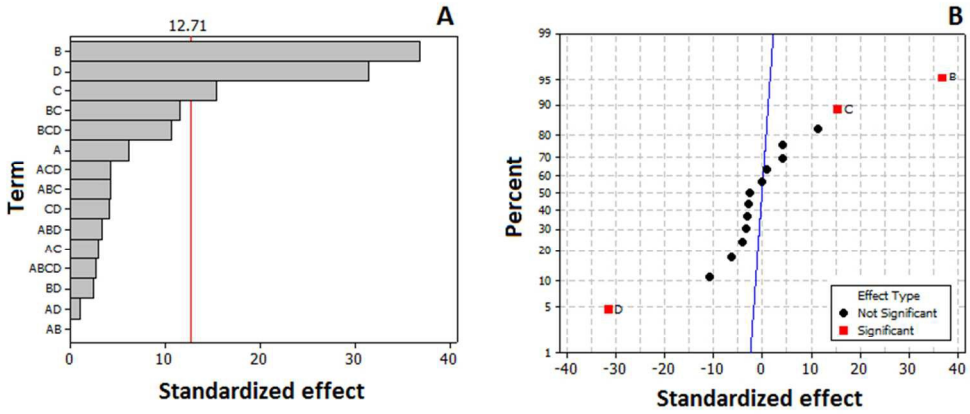

217x93mm (96 x 96 DPI)

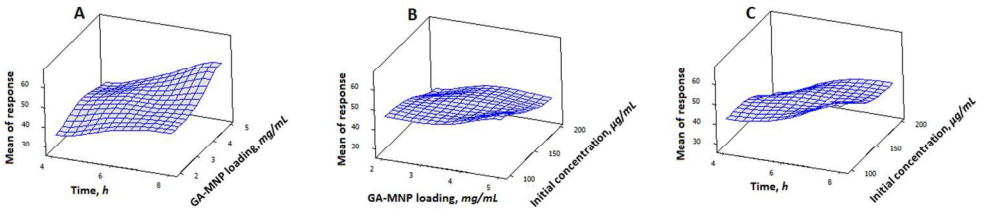

345x80mm (96 x 96 DPI)

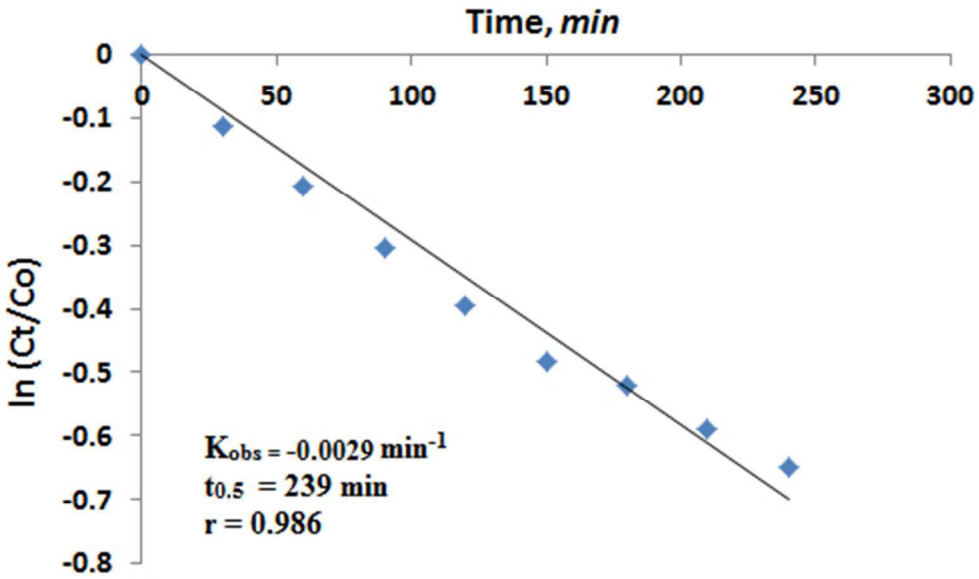

132x81mm (96 x 96 DPI)

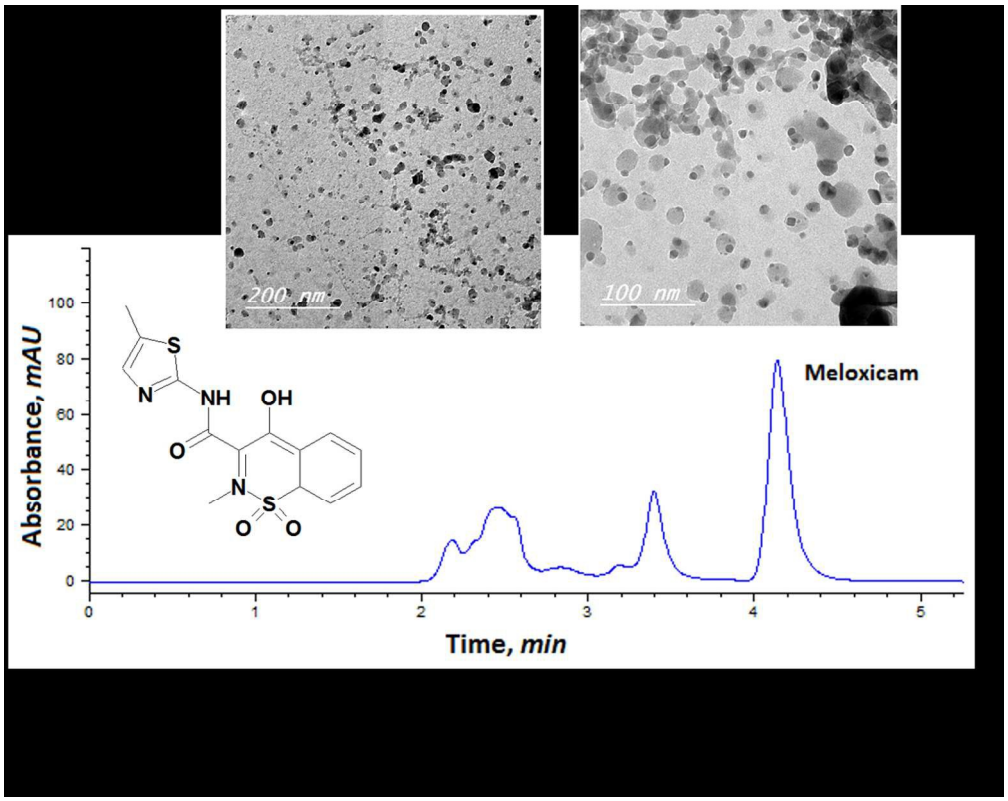

Graphical abstract
225x177mm (150 x 150 DPI)